

A QSO survey via optical variability and zero proper motion in the M 92 field

III. Narrow emission line galaxies

H. Meusinger^{*} and J. Brunzendorf^{*}

Thüringer Landessternwarte Tautenburg, D-07778 Tautenburg, Germany
e-mail: meus@tls-tautenburg.de, brunz@tls-tautenburg.de

Received 26 November 2001 / Accepted 13 May 2002

Abstract. We study a sample of 23 narrow-emission line galaxies (NELGs) which were selected by their strong variability as QSO candidates in the framework of a variability-and-proper motion QSO survey on digitised Schmidt plates. In previous work, we have shown that variability is an efficient method to find AGNs. The variability properties of the NELGs are however significantly different from those of the QSOs. The main aim of this paper is to clarify the nature of this variability and to estimate the fraction of AGN-dominated NELGs in this sample. New photometric and spectroscopic observations are presented, along with revised data from the photographic photometry. The originally measured high variability indices could not be confirmed. The diagnostic line-ratios of the NELG spectra are consistent with H II region-like spectra. No AGN could be proved, yet we cannot rule out the existence of faint low-luminosity AGNs masked by H II regions from intense star formation.

Key words. Galaxies: active – Galaxies: starburst – Galaxies: emission lines

1. Introduction

The variability of flux densities is a common property of high-luminosity AGNs. We have performed a QSO search based on variability and proper motion (VPM survey) measured on a large number of digitised Schmidt plates in two fields (Meusinger et al. 2002). The work in the M 92 field is the subject of the present series of papers. In the first paper (Brunzendorf & Meusinger 2001; hereafter Paper 1), we discussed the motivation, the observational data, the data reduction procedure, and the selection of QSO candidates. The results from the follow-up spectroscopy and the properties of the resulting QSO sample were the subject of Paper 2 (Meusinger & Brunzendorf 2001). The primary goal of the present study is to improve the understanding of the selection effects of this survey.

An object is considered a VPM-QSO candidate if it appears star-like, has no significant proper motion, and shows significant overall variability and long-term variability. The variability is expressed by the indices I_σ (overall variability) and I_Δ (long-term variability). For instance, an object with $I_\sigma > 2$ has a probability of $\alpha > 0.98$ to

be variable. It is well known that high-luminosity AGNs vary on long timescales (years and longer). High priority QSO candidates have therefore to meet both $I_\sigma \geq 2$ and $I_\Delta \geq 2$. On the other hand, we found several QSOs with strong overall variability but without significant long-term variability (Paper 2). The long-term variability constraint may introduce a bias in the VPM QSO search, and it is therefore important to study also the subsample of variable, star-like objects with zero proper motion showing no significant long-term variability. In particular, we found 27 narrow emission line galaxies (NELGs) with redshifts $z \lesssim 0.2$ in this subsample. Most of these galaxies show strong emission lines. NELGs may be dominated by narrow-emission line AGNs (Seyfert 2, narrow-emission line Seyfert 1, LINERs), intense starbursts, or a mixture of both. For example, Ho et al. (1997) found that about half of the NELGs from their magnitude-limited sample show some form of AGN or composite spectra. In Paper 2, we have speculated that at least some of the VPM NELGs are dominated by AGNs, though the available data did not allow a clear-cut conclusion.

The present paper is concerned with the sample of the NELGs from the VPM survey. The main question is whether the measured strong overall variability as well as the strong emission lines are related to AGNs or not. It is not our intention to provide a large and well-defined sam-

^{*} Visiting Astronomer, German-Spanish Astronomical Centre, Calar Alto, operated by the Max-Planck-Institute for Astronomy, Heidelberg, jointly with the Spanish National Commission for Astronomy

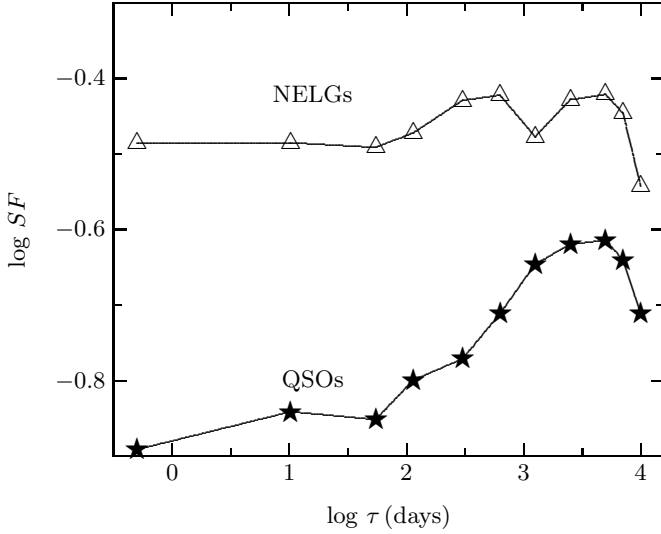


Fig. 1. Sample averaged structure function SF as a function of the time-lag τ in days for the NELGs (open triangles and upper polygon) and the QSOs (asterisks and lower polygon), respectively, from the VPM survey in the M 92 field.

ple of NELGs useful for further detailed studies. Much larger samples (e.g., Terlevich et al. 1991; Ho et al. 1997; Popescu & Hopp 2000) are available and are better suited to the investigation of the overall NELG population. In Sect. 2, we present new spectroscopic and photometric observations. Section 3 is concerned with the variability properties of the NELGs. The spectroscopic properties are discussed in Sect. 4, and Sect. 5 reviews further properties of the galaxy sample. Sect. 6 concludes. As in the previous papers of this series, we adopt $H_0 = 50 \text{ km s}^{-1} \text{ Mpc}^{-1}$ and $q_0 = 0$.

2. Observations and data reduction

Low resolution spectra of VPM QSO candidates were described in Paper 2. Unfortunately, the spectra for the NELGs did not allow a clear-cut separation between the principal ionisation sources (AGNs versus massive stars). New observations were performed with CAFOS at the 2.2 m telescope on Calar Alto, Spain, during six nights in July 2000. CAFOS was equipped with a SITeId CCD. The grism was chosen dependent on the redshift: low- z NELGs were observed with G-100 in order to achieve a good separation between $\text{H}\alpha$ and $[\text{N II}]\lambda 6583 \text{\AA}$. For the higher- z NELGs, G-200 was used because of its higher transmission at longer wavelengths. For some objects, spectra were taken with both grisms. Total integration times between 30 and 60 min were necessary to obtain spectra of reasonable signal-to-noise. The weather conditions were mainly good. The seeing was stable ($1''.0$ to $1''.2$) and the slit width was kept constant, resulting in a linear resolution of 10\AA (G-200) and 5\AA (G-100), respectively. The orientation of the slit was always North-South. Wavelength calibra-

tion spectra were taken by means of Hg-He-Ar calibration lamps.

We omitted two of the 27 NELGs that are located close to brighter galaxies since their measured variability is very likely not real. Further, the two NELGs of lowest priority could not be observed due to poor weather on the last night of the observing run. For the remaining 23 NELGs, spectra of good quality were obtained. In addition, six comparison galaxies with well-known spectroscopic data and spectral classification (see Table 3) were observed. All spectra were reduced on the basis of ESO-MIDAS routines, in particular the MIDAS package LONG. The resulting one-dimensional spectra are dominated by the emission from the central regions of the NELGs. The spectra were not flux-calibrated.

A subset of NELGs were photometrically monitored during the CAFOS campaign. We selected the 10 galaxies with highest variability indices and small deviations from a star-like image structure. On each of the six nights, we took a 180 s direct image of a $5' \times 5'$ field around each of the 10 galaxies through a Johnson B filter. The CCD frames were reduced using MIDAS standard routines.

3. Variability

The variability indices derived from the magnitude measurements in Paper 1 show two fundamental differences between NELGs and QSOs. First, there is no indication for significant long-term variability in the NELG sample, contrary to the QSOs. On the other hand, strong variability of the NELGs is indicated at short timescales of a few days or less. These differences are clearly illustrated by the comparison of the sample-averaged structure functions in Fig. 1 (for definitions and properties of the structure function see e.g. Simonetti et al. 1985). The absence of long-term variability is probably consistent with the presence of low-luminosity AGNs (LLAGNs) that are suspected to have shorter variability timescales than high luminosity AGNs (Filippenko 1992; Lira et al. 1999; Moran et al. 1999).

Strong variability on short timescales is provable by means of CCD time-series observations with a baseline of a few days. The results from our CCD-monitoring campaign do not indicate significant variability at the 0.02 mag level. We adopt the null-hypothesis $H_0 : \sigma_{B,\text{NELG}} = \sigma_{B,\text{star}}$, i.e. the photometric standard deviation σ_B is the same for the NELGs and the stars of comparable magnitude. The F test shows that H_0 should not be rejected on a significance level $\alpha = 0.95$ for 9 of the 10 NELGs. For the remaining object, the measured F is close to the critical value F_{crit} . Hence, there is no evidence of significant short-term variability from the CCD time-series.

The photographic photometry described in Paper 1 was based on a two-dimensional Gaussian profile-fitting procedure. Deviations of the image profile from the Gaussian leads to an increased measurement error and, combined with variations of the observing conditions from plate to plate, to artificial variability. This effect is clearly

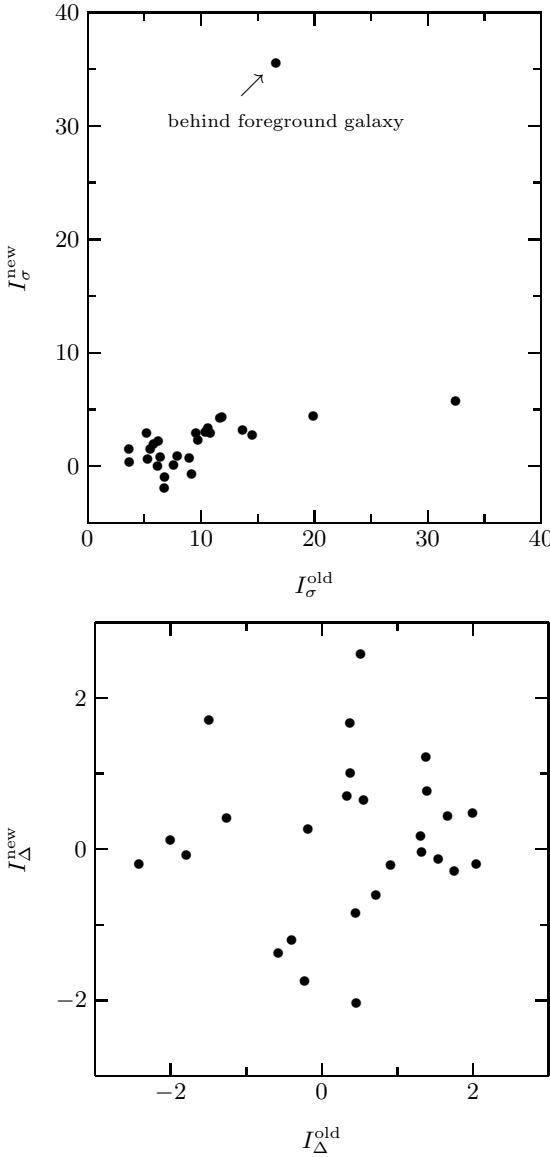


Fig. 2. New and old variability indices for the NELGs for overall variability (top) and long-term variability (bottom).

reflected by the high variability indices measured for galaxies with extended images. However, all but three NELGs appear star-like even on the deepest plates, and none of the NELGs was classified as extended on the basis of the index $I_{\text{nonstellar}}$.

In order to solve the discrepancy between the strong variability from the Schmidt plate data and the results of the CCD time-series, we have completely revised the reduction of all 162 B Schmidt plates. The SExtractor package (Bertin & Arnouts 1996) was used and magnitudes were measured by aperture photometry instead of profile fitting. At the faint end, the photometric accuracy of the revised data is improved by a factor of about two. An additional improvement is achieved by averaging the measured magnitudes of an object over adjacent epochs. This was done if (a) the single-epoch data have

too low a photometric accuracy, i.e. $\sigma_B(B = 19^m) > 0.1$ or $\sigma_B(B = 20^m) > 0.2$, and (b) there are several plates available of close-by epochs. Thus, we finally have 54 data points of different epochs spanning 33.2 years. For each individual epoch, the photometric accuracy is better than 0.1 mag at $B = 19$ and better than 0.2 mag at $B = 20$. This is a significant improvement compared to the original data (cf. Fig. 5 in Paper 1).

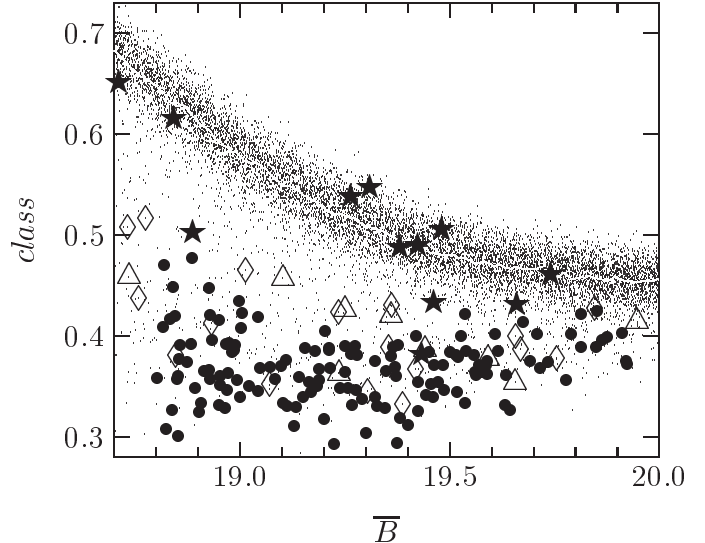


Fig. 3. The new object classification parameter $class$ for all objects (dots) in the magnitude range of the NELGs. The white curve represents the running median, the various symbols designate visually identified galaxies (bullets), Seyfert 1 galaxies with $z \leq 0.5$ (asterisks), and NELGs (open lozenges for $M_B < -20$, open triangles for $M_B > -20$), respectively.

The variability indices I_{σ} and I_{Δ} were computed in exactly the same way as in Paper 1. In Fig. 2, we compare the new with the old variability indices of the NELGs. The values are listed in Table 1, along with the other photometric data. As for the original data, no significant long-term variability is found from the revised data. The overall variability indices from the revised photometry are considerably reduced: only about 50% of the NELGs have $I_{\sigma}^{\text{new}} > 2$. An outstandingly high $I_{\sigma}^{\text{new}} \approx 35$ is found for an NELG that is projected onto an extended foreground galaxy. These facts illustrate that the way of measuring magnitudes is of major importance for the assessment of variability.

In Paper 1, image profile indices were derived from the radius-magnitude relation. The SExtractor package allows a more sophisticated morphological classification based on a trained neural network. According to the classification parameter $class$ derived by SExtractor, NELGs are clearly separated from star-like objects (Fig. 3). On the other hand, the classification parameters of some of the Seyfert galaxies from the VPM survey are similar

Table 1. Photometric data for the 23 NELG sample of the present study. The running number, J2000.0 position, mean B magnitude, mean absolute magnitude M_B (with redshift from Table 2), old and new overall variability indices I_σ and I_Δ , new morphology index I_{nst} (where “nst” means “nonstellar”), as well as the mean colour indices $U - B$ and $B - V$ (without reddening correction, without k correction) are given.

no.	NELG	\overline{B}	M_B	I_σ^{old}	I_Δ^{old}	I_σ^{new}	I_Δ^{new}	$I_{\text{nst}}^{\text{new}}$	$U - B$	$B - V$
1	J171122.0+440721	19.4	-20.5	5.53	0.33	1.44	0.69	3.7	-0.45	0.80
2	J171124.1+433117	19.7	-21.0	5.19	-0.57	2.87	-1.38	5.1	-1.38	0.29
3	J171241.1+430512	19.4	-21.0	13.66	-2.00	3.11	0.11	6.7	-0.17	1.10
4	J171319.5+435216	19.1	-20.6	11.68	1.54	4.20	-0.14	10.8	-0.90	0.38
5	J171323.0+431230	18.7	-20.6	9.19	1.75	-0.72	-0.29	8.7	-0.33	0.65
6	J171326.8+440117	19.1	-17.1	6.16	0.91	-0.03	-0.22	4.7	-0.52	0.76
7	J171448.3+434455	18.8	-20.7	8.96	0.37	0.69	1.66	7.4	-0.24	0.43
8	J171459.0+434327	19.4	-18.4	7.57	1.38	0.07	1.21	5.6	-0.07	0.85
9	J171510.7+430506	19.4	-20.1	6.41	1.30	0.74	0.17	8.9	-0.63	1.15
10	J171520.1+433427	18.7	-19.5	10.61	-0.22	3.32	-1.75	11.3	-0.25	0.66
11	J171610.9+422333	18.8	-21.6	32.47	0.45	5.70	-2.05	12.0	-0.50	1.06
12	J171652.4+433528	19.7	-18.1	6.26	2.04	2.11	-0.21	7.2	-0.12	0.51
13	J171734.2+432824	19.9	-18.8	7.92	1.31	0.87	-0.04	2.9	-0.79	0.67
14	J171734.9+425643	19.8	-20.3	6.78	-0.18	-1.00	0.26	2.0	-0.62	0.73
15	J171747.3+432550	19.2	-18.8	10.82	0.44	2.85	-0.86	8.2	-0.52	1.05
16	J171828.1+442727	19.4	-18.8	5.82	-1.49	1.89	1.71	4.2	-0.44	0.65
17	J171908.9+423111	19.3	-21.0	10.37	1.39	2.97	0.77	8.8	-0.76	1.06
18	J171955.6+442244	18.9	-20.4	11.85	-1.25	4.23	0.41	9.7	0.34	0.62
19	J172156.0+441912	19.3	-17.0	6.74	-1.79	-2.02	-0.08	4.8	-0.71	0.53
20	J172256.1+425447	19.4	-21.2	9.76	0.51	2.28	2.57	6.0	-0.64	1.17
21	J172340.6+434102	19.6	-19.4	14.51	-2.41	2.66	-0.20	5.8	-0.19	0.56
22	J172348.1+432907	19.0	-21.4	9.54	-0.40	2.86	-1.21	5.5	-1.01	0.93
23	J172407.6+424037	19.2	-21.3	3.65	0.55	1.46	0.65	5.0	-0.75	0.69

to NELGs. Analogously with the nonstellar index from Paper 1, we define a new nonstellar index

$$I_{\text{nonstellar}}^{\text{new}} = \frac{\overline{\text{class}} - \overline{\text{class}(B)}}{\sigma_{\text{class}}(B)},$$

where $\overline{\text{class}}(B)$ is the median of the classification parameter of all objects at magnitude B , and $\sigma_{\text{class}}(B)$ is the standard deviation. Figure 4 clearly shows that the objects with higher (new) nonstellar indices tend to have higher (new) variability indices. This correlation strongly suggests that the measured large variability indices of the NELGs are dominated by measurement errors due to the deviations from stellar appearance.

4. Spectral classification

The spectra cover the wavelength interval between about 4800 Å and 8200 Å in the observer frame. Prominent lines are H β , [O III] $\lambda 5007$, [O I] $\lambda 6300$, H α , [N II] $\lambda 6583$, and the [S II] $\lambda\lambda 6717, 6731$ blend. The accuracy of the emission line equivalent widths (EWs) is determined primarily by the uncertainty in the level of the continuum. The problem of a subjective bias was partly overcome by a non-interactive measurement procedure. Briefly, the level of the local continuum is estimated by means of median and low-pass filters. Then, the EW is estimated at the position calculated from the previously measured redshift. The redshifts and the resulting EWs are listed in Table 2. The errors given

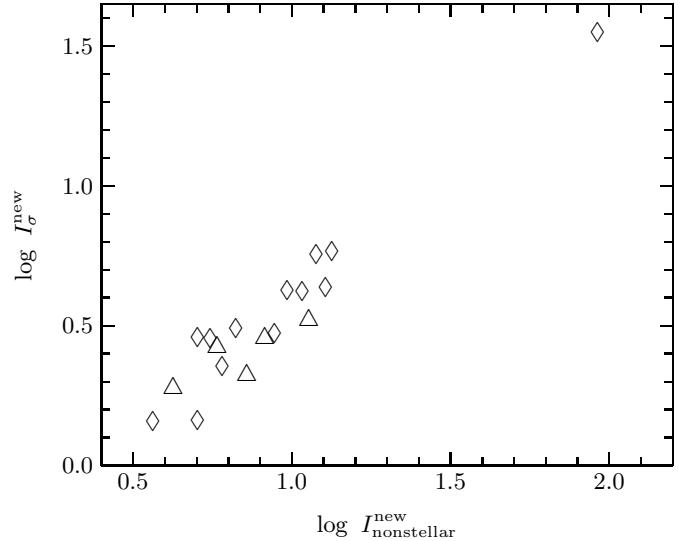


Fig. 4. Overall variability index I_σ^{new} versus image profile index $I_{\text{nonstellar}}^{\text{new}}$ from the revised photometry for the NELGs with significant variability, i.e. $I_\sigma^{\text{new}} > 1$. (Symbols as in Fig. 3.)

there are the random errors derived by the measuring procedure. In general, the Balmer lines will be blended. We follow the approach by Popescu & Hopp (2000) to correct for the absorption by the underlying older stellar population: for all galaxies with strong continuum emission

($EW(H\beta) < 20 \text{ \AA}$) the measured $EW(H\beta)$ is increased by an assumed constant absorption EW. A constant value of $EW_{\text{abs}}(H\beta) \approx 2 \text{ \AA}$ was found by McCall et al. (1985) and is in good agreement with the data given by Ho et al. (1997). $H\alpha$ absorption was corrected for in the same way with $EW_{\text{abs}}(H\alpha) \approx 1.7 \text{ \AA}$ derived from the Ho et al. sample.

It is a common practice to discriminate between AGNs and massive stars by means of line-ratio diagrams (Baldwin et al. 1981; Vieilleux & Osterbrock 1987; Ho et al. 1997). We use the diagnostic line-ratios recommended by Vieilleux & Osterbrock that are based on the measurements of the lines mentioned above. Since the wavelength separation of the considered lines are small, these line-ratios are relatively insensitive to reddening (cf. Dessauges-Zavadsky et al. 2000). Line-ratios are expressed by the ratios of the corresponding EWs. Figure 5 shows these diagnostic diagrams for all galaxies. Each object was individually classified on each of the three diagrams, and then the consistency of the three classifications was evaluated. We consider three spectral classes: H II galaxies to the left of the demarcation curves, AGNs to the right, and transition objects near the boundary (i.e., the error bars cross the demarcation). In addition, we define two classification types: unambiguous (u), i.e. all relevant data are consistent with one spectral class, or ambiguous (a), i.e. the object is classified both as AGN and H II galaxy on different diagrams. The results are given in Table 2. For ambiguous classifications the two most likely classes are given. There is good agreement between the spectral classes derived for the six comparison galaxies and the classification from the literature (Table 3).

The results can be summarised as follows: for most of the NELGs the line-ratios correspond to H II region spectra. None of the NELGs is unambiguously classified as an AGN. Only for one object is more than one diagram compatible with an AGN spectrum, but the signal-to-noise is relatively low in this case. A substantial fraction of the sample (40%) has an ambiguous classification, and a similar fraction is located near the H II-AGN border. It must be emphasised that the line-ratios are derived from integrated spectra. At a redshift of $z = 0.1$, a slit width of $1''$ covers about 2 kpc. In the direction of the long-slit, the spectrum integrates over the whole galaxy. For many of the NELGs rotation curves are seen in $H\alpha$ indicating the presence of extended emission regions like circum-nuclear rings or spiral arms. If an LLAGN is present, it can thus be masked by the emission from H II regions connected to intense star formation (Storchi-Bergmann et al. 1996; Pastoriza et al. 1999). A trend of decreasing line ratios with increasing effective aperture, and therewith with increasing z , is expected if AGNs substantially contribute to the spectra (Storchi-Bergmann 1991). Such a trend is not indicated in our data. We cannot exclude that there are LLAGNs in at least some of the NELGs. However, the integrated spectra are not dominated by AGNs.

5. Further properties of the NELG sample

Some trends with $EW(H\alpha)$ are shown in Fig. 6 (where NELG 19 with its exceptionally high EWs was excluded for the sake of clearness). There is a strong correlation between $EW(H\beta)$ and $EW(H\alpha)$. The slope is similar to that of nearby galaxies and implies a mean extinction $A_V \approx 1 \text{ mag}$ (cf. Kennicutt 1992). Further, there are loose correlations with $EW(H\alpha)$ for the EWs of the lines $[\text{O III}]\lambda 5007$, $[\text{N II}]\lambda 6583$, and $[\text{S II}]\lambda\lambda 6717, 6731$. Such trends are known from samples of nearby galaxies (e.g., Tresse et al. 1999; Sodré & Stasińska 1999). The large dispersions are likely due to the variation in the mean nebular excitation in the galaxies (Kennicutt 1992).

Our sample is magnitude-limited and the absolute magnitudes are therefore strongly correlated with redshifts. Further, due to the constraint of star-like images, the characteristic scale-length of the dominant component is of the order of a few arcseconds or less. The sample thus comprises roughly two classes of objects: dwarfs and sub- L^* galaxies at $z < 0.1$ and $\sim L^*$ galaxies at $0.1 \lesssim z \lesssim 0.2$. These two subclasses are marked by different symbols in all relevant figures. The most significant difference between the sub- L^* and the $\sim L^*$ galaxies are the mean EWs (Fig. 6, bottom): NELGs with fainter absolute magnitudes show a clear tendency to have smaller $EW(H\alpha)$. This trend is opposite to what is found in a representative sample of galaxies in the local universe (Tresse et al. 1999). If the trend in Fig. 6 is real, it is probably related to the selection effects of the VPM search. However, a plausible explanation for this trend has not yet been found.

Most of the NELGs are blue (Table 1). Using the K corrections for Sbc galaxies (Coleman et al. 1980), the corrected sample-averaged colour indices are $\langle U - B \rangle = -0.66 \pm 0.37$ and $\langle B - V \rangle = 0.48 \pm 0.25$. (The $U - B$ colour is probably slightly underestimated due to a bias towards brighter magnitudes at the faint end of the U measurements.) The blue colours are likely a selection effect: the object selection is based on the morphological classification done on the deepest red plate and on the variability measured on B plates (Paper 1). Galaxies that are compact on the red plate but more extended, and therewith brighter on the blue plates, have therefore a good chance to be selected as (nearly) star-like and variable objects. The M_B distribution of the NELGs is similar to that of galaxies selected for their compact nuclei (Sarajedini et al. 1999).

The $EW(H\alpha)$ vs. $B - V$ diagram for the NELGs of the present study (Fig. 7) resembles the one for the starburst galaxies discussed by Moy et al. (2001). According to these authors, the most attractive explanation for this diagram is provided by galaxy models with continuous star formation + starbursts where the ages and metallicities of the underlying population are similar to those in normal spirals.

Direct 100 s exposures were obtained in the V band for all 23 NELGs. There is little information about morphological details for most of the galaxies. Deeper im-

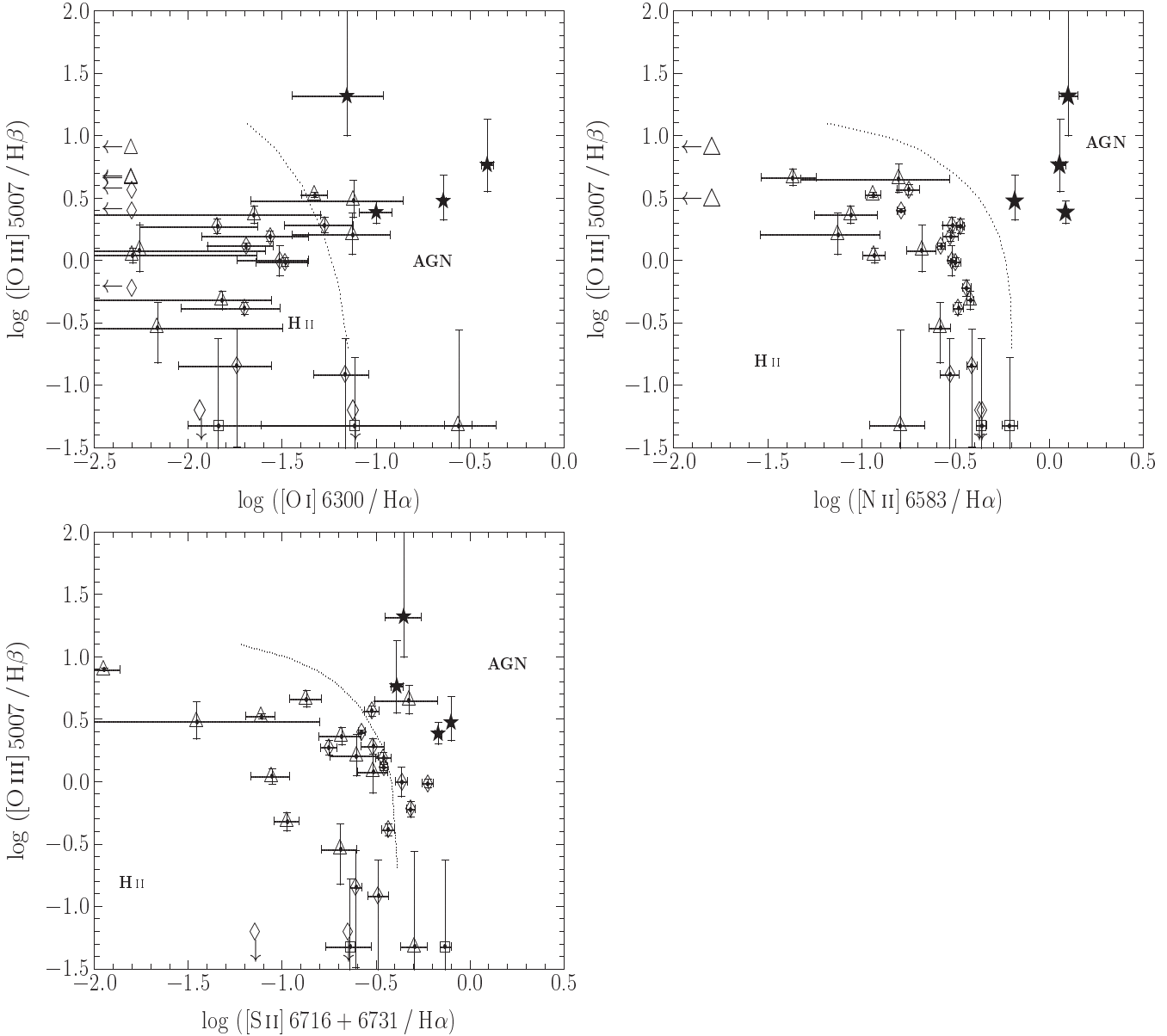


Fig. 5. Diagnostic line-ratio diagrams for the NELGs (symbols as in Fig. 3) and the comparison galaxies (galaxies classified in the literature as Seyferts or LINERs are marked as asterisks, transition types as open boxes).

ages are available for the 10 NELGs from the photometric series where six 180 s B band exposures for each object were co-added. Since we are interested in the extended, non-star-like structure components, the images were PSF-deconvolved applying the Lucy-Richardson algorithm. The resulting images (Fig. 8) show that all NELGs have dominant, more or less compact components. In addition, a more extended fainter component is indicated in many cases. Structure details like spiral arms, bars, or rings cannot be recognised. Some NELGs (4, 11, 19) clearly show asymmetric light distributions, perhaps indicating morphological distortions. Many of the NELGs have several close-by neighbour galaxies (in projection). For instance, NELG 11 seems to be a highly disturbed

galaxy in the centre of a group, and the dwarf NELG 13 seems to have a light-bridge toward a nearly edge-on giant spiral at a projected distance of less than 20 kpc. A further interesting object is NELG 19 which is probably a cometary blue compact dwarf galaxy with EWs similar to Mkn 71 (for the latter, see Kennicutt 1992; Noeske et al. 2000).

The VPM NELGs have properties characteristic of starbursts and are thus expected to be strong emitters in the far infrared (FIR). There are no entries in the NED¹ at the positions of the NELGs, and there are

¹ The NASA/IPAC Extragalactic Database (NED) is operated by the Jet Propulsion Laboratory, California Institute of

Table 2. Spectroscopic data for the NELG sample of the present study. Running numbers from Table 1, used grism, redshift z , measured equivalent widths (in Å) of the major emission lines, and the results of the spectral classification are given. For ambiguous classifications the two most likely classes are given with the most probable one at the first position. Classifications from spectra with relatively low signal-to-noise ratio have a questionmark.

no.	grism	z	H β 4861 Å	[O III] 5007 Å	[O I] 6300 Å	H α 6565 Å	[N II] 6584 Å	[S II] 6716/31 Å	spectral class
1	G100	0.1457	14.2±0.6	6.7±0.5	1.5±0.8	75.4±1.0	24.7±1.2	27.6±1.7	H II
2	G200	0.2087	30.7±0.6	77.0±0.7	0.1±1.2	171.5±1.1	27.8±1.2	45.5±1.7	H II
3	G200	0.1867	2.1±0.3	0.5±0.4	2.3±0.7	33.6±0.9	9.9±0.9	10.9±1.1	H II
4	G200	0.1362	22.3±0.8	74.5±0.9	6.1±0.9	129.1±1.3	14.9±1.3	10.0±1.7	H II
5	G100	0.1150	4.1±0.6	11.7±0.5	1.9±0.7	35.7±1.1	10.8±1.0	10.9±1.2	H II
6	G100	0.0270	5.5±2.2	9.0±1.1	0.2±0.7	36.3±1.2	7.6±1.1	11.1±1.7	H II
6	G200	0.0275	7.9±0.7	10.9±0.7	0.2±0.7	39.5±0.6	4.6±0.6	3.5±0.8	H II
7	G100	0.1265	13.6±0.7	15.1±0.6	2.4±0.7	72.9±1.2	23.0±1.1	43.5±2.4	H II, (AGN)
8	G100	0.0576	3.8±1.4	9.3±1.2	1.6±0.8	21.3±1.1	1.6±1.0	5.3±1.3	H II,(T) ?
9	G100	0.1256	3.8±0.7	0.1±0.8	0.3±0.6	25.7±1.0	10.9±0.9	5.8±1.7	H II
10	G100	0.0690	2.4±1.0	0.0±0.7	2.3±0.7	29.6±1.0	12.9±1.0	2.1±1.1	H II
10	G200	0.0690	3.4±0.3	2.6±0.3	0.5±0.4	33.0±0.4	12.5±0.4	3.5±0.5	H II,(T) ?
11	G200	0.1824	0.8±0.3	0.4±0.3	0.6±0.3	33.1±0.6	12.8±0.6	8.2±0.5	H II
12	G200	0.0576	0.1±0.3	0.1±0.4	2.4±0.3	7.0±0.4	1.4±0.4	4.4±0.5	AGN,(H II) ?
13	G100	0.0892	0.8±0.6	12.5±0.5	0.0±0.4	2.1±0.4	0.6±0.4	1.8±0.5	H II,(AGN) ?
14	G100	0.1698	10.0±0.6	18.7±0.7	1.8±1.0	65.9±1.7	19.6±1.4	22.8±1.5	H II, (T)
15	G100	0.0655	10.2±1.4	28.2±1.2	1.0±1.2	44.6±1.4	3.9±1.3	9.3±2.1	H II
15	G200	0.0659	4.6±0.8	30.3±0.8	0.1±0.6	48.7±0.7	2.1±0.7	6.6±1.2	H II
16	G100	0.0680	3.3±1.4	16.0±1.2	1.3±0.9	15.4±1.4	0.0±1.3	0.6±1.9	H II,(AGN) ?
17	G200	0.1828	8.6±0.9	19.9±1.0	1.8±1.1	125.7±1.5	42.2±1.5	22.4±1.9	H II
18	G200	0.1147	2.4±0.6	4.4±0.6	1.5±0.6	48.9±0.6	14.8±0.6	21.2±1.3	H II,(AGN)
19	G200	0.0278	229.8±4.1	1813.8±2.6	0.7±2.2	1066.7±2.0	10.2±1.9	12.1±2.6	H II
20	G200	0.2051	5.3±0.4	4.4±0.4	0.1±0.7	52.3±0.8	18.9±0.8	25.3±1.0	H II,(AGN)
21	G100	0.1002	4.6±0.7	1.9±0.8	0.2±0.7	29.1±0.8	7.6±0.8	6.0±1.1	H II
22	G200	0.1871	8.4±0.3	13.6±0.4	1.6±0.6	78.3±0.8	20.8±0.8	27.2±0.9	H II
23	G200	0.2056	7.2±0.7	33.9±0.7	0.1±1.4	76.0±1.7	13.6±1.6	22.8±1.7	H II

Table 3. Spectroscopic data for the set of six comparison galaxies. The grism used, the measured equivalent widths (in Å) of the major emission lines, the results of the spectral classification (S: Seyfert, L: LINER, T: transition type), and the classification type (u: unambiguous, a: ambiguous) are given. For comparison, spectral types from the literature are given (references: (1) Ho et al. 1997, (2) Greenhill et al. 1997).

galaxy name	grism	H β 4861 Å	[O III] 5007 Å	[O I] 6300 Å	H α 6565 Å	[N II] 6584 Å	[S II] 6716,6731 Å	class (here)	class. type	class (lit)
NGC3031	G100	0.0±1.1	11.6±0.5	5.3±0.2	11.8±0.5	15.4±0.4	5.5±0.2	S	u	S ¹
NGC3031	G200	0.1±1.7	8.9±0.4	5.4±0.2	19.8±0.2	20.3±0.2	5.1±0.2	S	u	S ¹
NGC5678	G200	0.1±0.3	0.1±0.2	0.3±0.2	2.2±0.2	2.4±0.1	0.9±0.2	T	u	T ¹
NGC6323	G100	0.0±1.9	41.5±2.3	1.1±0.5	14.0±1.0	19.8±1.0	7.0±1.1	S	u	S ²
NGC6323	G200	1.9±1.2	31.6±0.6	1.4±0.3	22.0±0.4	21.2±0.4	6.1±0.4	S	u	S ²
NGC6500	G200	2.7±1.7	14.0±0.4	10.5±0.3	45.8±0.2	29.9±0.2	36.4±0.3	L,(S)	a	L ¹
NGC7177	G200	0.1±0.4	0.1±0.3	0.1±0.2	5.2±0.2	3.0±0.1	5.1±0.2	T?	a	T ¹
NGC7743	G200	0.1±0.3	5.1±0.3	1.1±0.2	9.2±0.2	13.3±0.2	7.4±0.2	T,(S)	u	S ¹

no IRAS counterparts. The latter is simply explained by the IRAS detection limits: galaxies with $B \approx 19$ must have $\log L_{\text{FIR}}/L_B > 1.7$ to be found in the IRAS catalogues. Such a strong FIR excess is characteristic of only a few ultra-luminous IR galaxies (Sanders & Mirabel 1996)

which have much stronger internal extinction in the optical than is indicated for the NELGs (Fig. 6).

6. Conclusions

We have studied the sample of NELGs from the VPM survey in the M92 field. These objects have been selected as QSO candidates because of their high variability indices (Paper 1) and have been classified later as NELGs

Technology, under contract with the National Aeronautics and Space Administration.

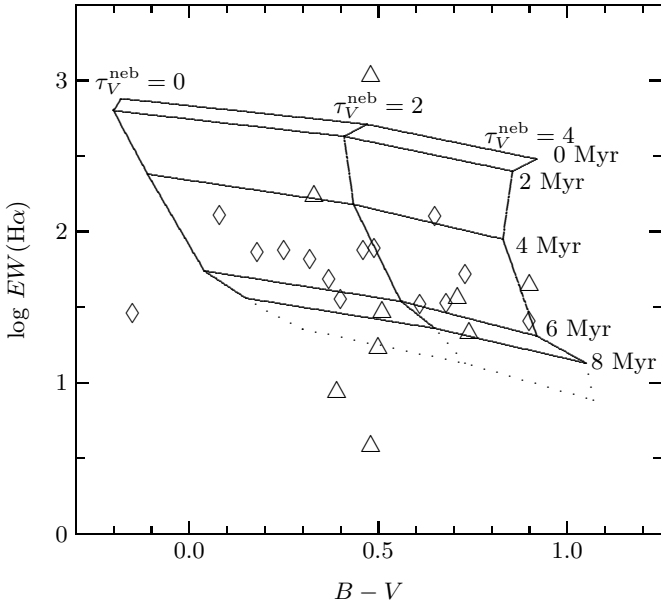


Fig. 7. $EW(H\alpha)$ versus $B - V$ for the NELGs (symbols as in Fig. 3). The solid lines show the predictions of model D by Moy et al. (2001; their Fig. 10) for continuous star formation + starbursts of different ages (labeled to the right of the grid) and extinction levels (labeled by the optical depth τ_V^{neb} at the top of the grid) for metallicity $Z = 1/2 Z_\odot$. The dotted lines show the shift of the low part of the grid for $Z = 3/2 Z_\odot$.

(Paper 2). However, it was not clear from the previous data to what extent the variability and the spectral properties of the NELGs are related to AGNs. In the present paper, we re-investigated the variability and analysed the emission line-ratios, as well as the photometric and morphological properties of the NELGs. The main conclusions are the following.

- The variability indices reported in Paper 2 primarily reflect increased measurement errors due to the resolved image profiles and do not provide evidence for AGNs. The measurement of variability for resolved objects requires techniques other than Gaussian profile fitting, even when the deviations from the stellar profiles are small. An unambiguous separation between stellar and nonstellar objects is crucial for the VPM survey.
- The diagnostic line-ratio diagrams are best explained by H II region-like spectra. None of the NELGs is unambiguously classified as an AGN. At least for some of the NELGs, the existence of LLAGNs cannot be excluded. However, if present, AGNs do not dominate the integrated spectra.
- The VPM NELGs are compact, blue galaxies. Most of them are related to starbursts. The sample consists of a range of various types, as is known from other samples of local starburst galaxies (e.g., Coziol et al. 1998).

An important result of this work is the substantial improvement of both the photometric accuracy and the star-galaxy separation for the objects from the VPM survey in the M 92 field. This enabled us to identify additional VPM-QSO candidates with high or medium priority in our sample. Their spectroscopic observations, the newly detected QSOs and the properties of the enlarged QSO sample will be the subject of Paper 4 of this series.

Acknowledgements. This research is based on observations made with the 2.2m telescope of the German-Spanish Astronomical Centre, Calar Alto, Spain. We acknowledge financial support from the *Deutsche Forschungsgemeinschaft* under grants Me1350/8 and /10. This research has made use of the NASA/IPAC Extragalactic Database (NED) which is operated by the Jet Propulsion Laboratory, California Institute of Technology, under contract with the National Aeronautics and Space Administration.

References

- Bertin, E., & Arnouts, S. 1996, A&AS 117, 393
 Baldwin J.A., Phillips, M.M., & Terlevich, R. 1981, PASP 93, 5
 Brunzendorf, J., & Meusinger, H. 2001, A&A 373, 38 (Paper 1)
 Coleman, G.D., Wu, C.C., & Weedman, D.W. 1980, ApJS 43, 393
 Coziol, R., Torres, C.A.O., Quast, G.R., et al. 1998, A&A 345, 733
 Dessauges-Zavadsky, M., Pindao, M., Maeder, A., et al. 2000, A&A 355, 89
 Filippenko, A.V. 1992, in ASP Conference Series 31, Relationships between active galactic nuclei and starburst galaxies, ed. A.V. Filippenko, p. 253
 Greenhill, L.J., Herrnstein, J.R., Moran, J.M., et al. 1997, ApJ 486, L15
 González Delgado, R.M., & Pérez, E. 1996, MNRAS 281, 1105
 Ho, L.C., Filippenko A.V., & Sargent, W.L.W. 1997, ApJS 112, 315
 Kennicutt, R.C. 1992, ApJ 388, 310
 Lira, P., Lawrence, A., O'Brien, P., et al. 1999, MNRAS 305, 109
 McCall M. L., Rybski, P. M., & Shields, G. A. 1985, ApJS 75, 1
 Meusinger, H., & Brunzendorf, J. 2001, A&A 374, 878 (Paper 2)
 Meusinger, H., Brunzendorf, J., Scholz, R.-D., et al. 2001, in ASP Conference Series, AGN Surveys, ed. R.F. Green, E.Ye. Khachikian, & D.B. Sanders, in press
 Moran, E.C., Filippenko, A.V., Ho, L.C., et al. 1999, PASP 111, 969
 Moy, E., Rocca-Volmerange, B., & Fioc, M. 2001, A&A 365, 347
 Noeske, K.-G., Guseva, N.G., Fricke, K.J., et al. 2000, A&A 361, 33
 Pastoriza, M.G., Donzelli, C.J., & Bonatto, C. 1999, A&A 347, 55
 Popescu, C. C., & Hopp, U. 2000, A&AS 142, 247
 Sanders, D.B. & Mirabel, I.F. 1996, ARA&A 34, 749
 Simonetti, J.H., Cordes J.M., & Heeschen D.S. 1985, ApJ 296, 46
 Sarajedini, V.L., Green, R.F., Griffiths, R.E., et al. 1999, ApJ 524, 746

- Sodré, L. & Stasińska, G. 1999, A&A 345, 391
Spiegel, M.R. 1990, Statistik, McGraw-Hill Book Company
Europe
Storchi-Bergmann, T., Wilson, A.S., & Baldwin, J.A. 1996,
ApJ 435, L105
Storchi-Bergmann, T. 1991, MNRAS 249, 404
Terlevich, R., Melnick, J., Masegosa, J. et al. 1991, A&AS 91,
285
Tresse, L., Maddox, S., Loveday, J., et al. 1999, MNRAS 310,
262
Vielleux S., & Osterbrock D.E. 1987, ApJS 63, 295

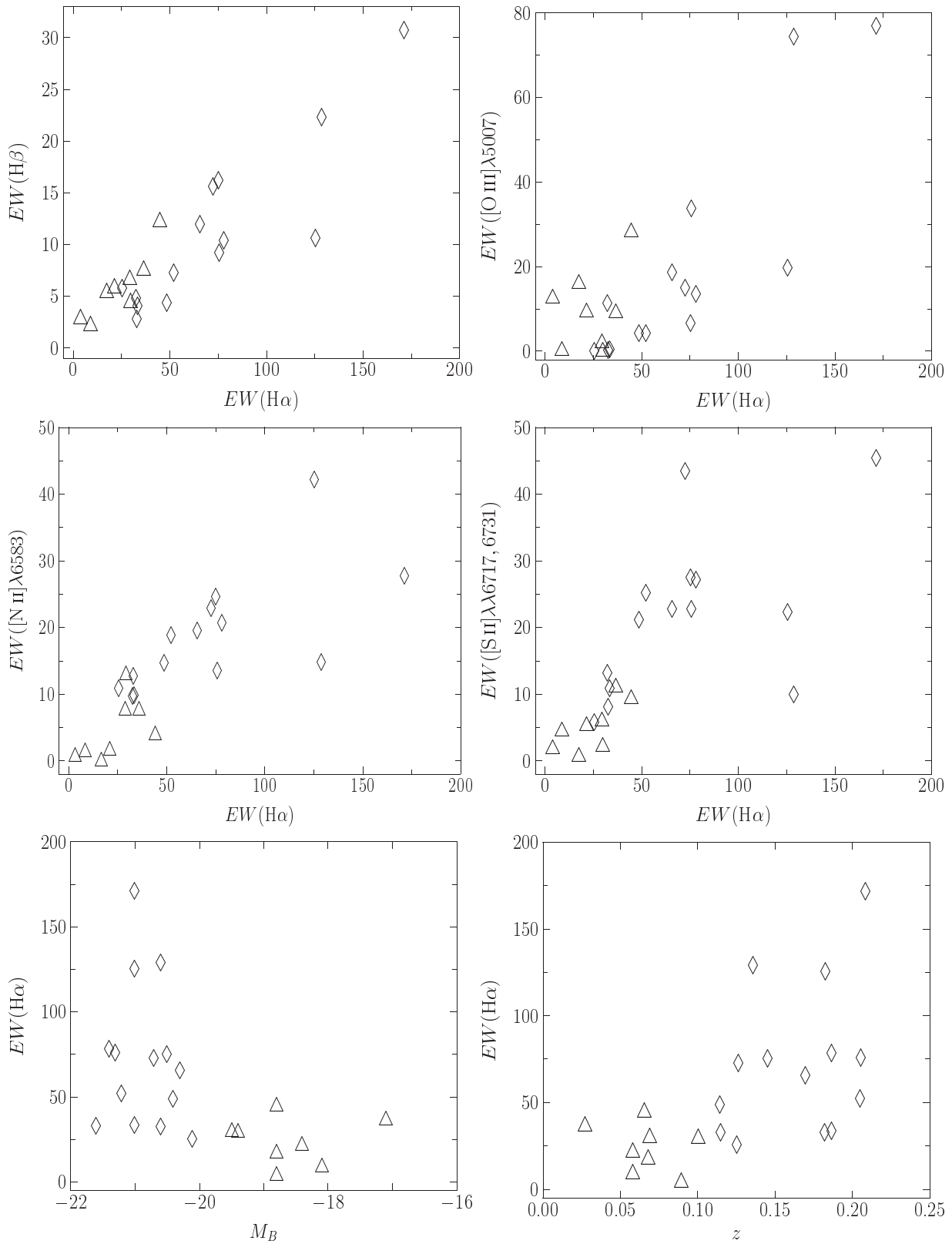


Fig. 6. Correlations with $EW(H\alpha)$. Symbols as in Fig. 3.

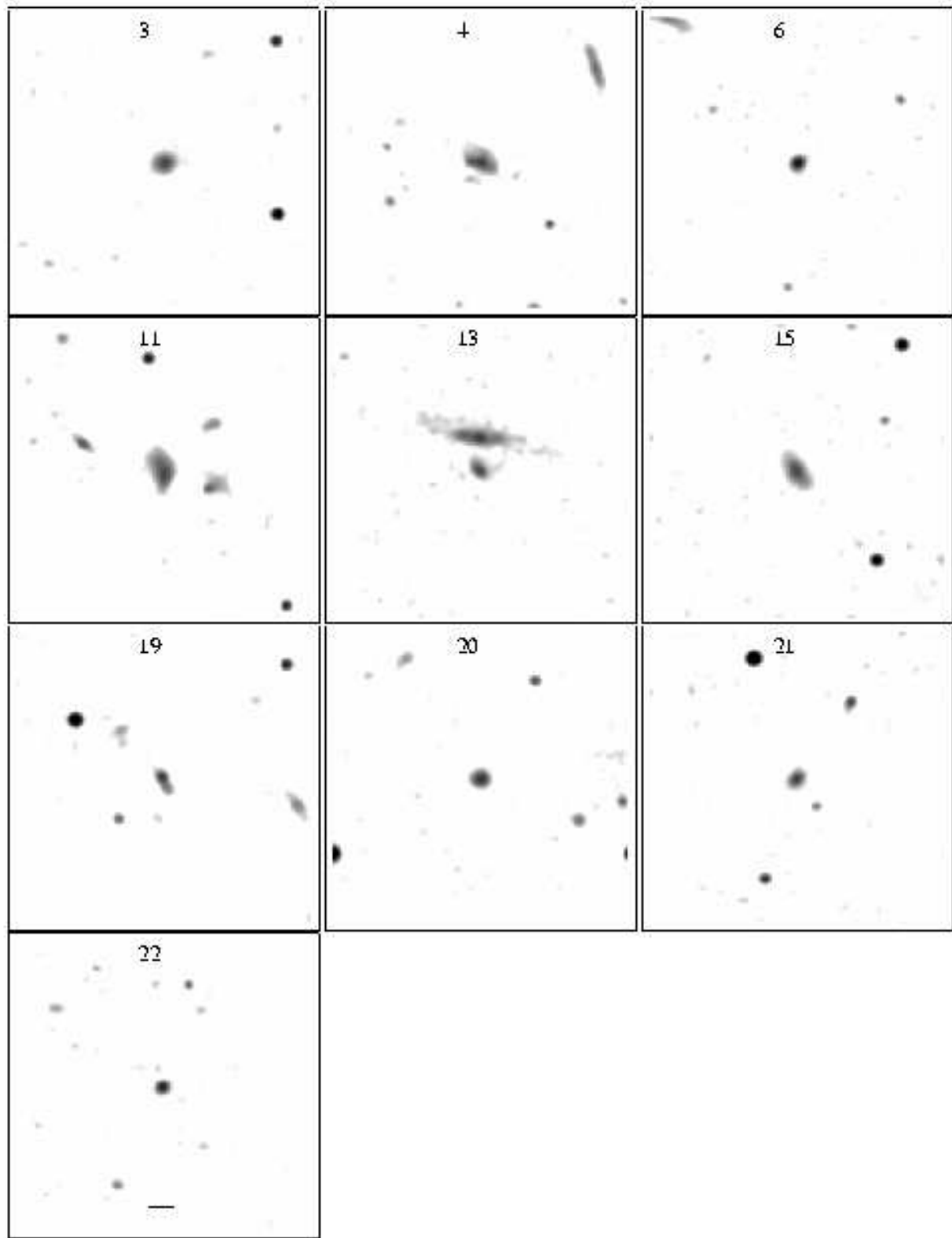


Fig. 8. Logarithmic gray scale presentation of 10 NELGs (in the middle of each panel) in the *B* band after Lucy-Richardson deconvolution. The image size is $1' \times 1'$, the horizontal line indicates 20 kpc at the distance of the galaxy. The panel numbers correspond to the running numbers of the NELGs from Table 1. N is up, E is right.